

In the format provided by the authors and unedited.

# Facet-dependent active sites of a single Cu<sub>2</sub>O particle photocatalyst for CO<sub>2</sub> reduction to methanol

Yimin A. Wu<sup>1,2</sup>, Ian McNulty<sup>1</sup>, Cong Liu<sup>3</sup>, Kah Chun Lau<sup>4,5</sup>, Qi Liu<sup>6</sup>, Arvydas P. Paulikas<sup>4</sup>, Cheng-Jun Sun<sup>7</sup>, Zhonghou Cai<sup>7</sup>, Jeffrey R. Guest<sup>1</sup>, Yang Ren<sup>7</sup>, Vojislav Stamenkovic<sup>4</sup>, Larry A. Curtiss<sup>4</sup>, Yuzi Liu<sup>1\*</sup> and Tijana Rajh<sup>1\*</sup>

---

<sup>1</sup>Center for Nanoscale Materials, Argonne National Laboratory, Argonne, IL, USA. <sup>2</sup>Department of Mechanical and Mechatronics Engineering and Waterloo Institute for Nanotechnology, University of Waterloo, Waterloo, Ontario, Canada. <sup>3</sup>Chemical Sciences and Engineering Division, Argonne National Laboratory, Argonne, IL, USA. <sup>4</sup>Materials Science Division, Argonne National Laboratory, Argonne, IL, USA. <sup>5</sup>Department of Physics and Astronomy, California State University, Northridge, CA, USA. <sup>6</sup>Department of Physics, City University of Hong Kong, Hong Kong, China. <sup>7</sup>Advanced Photon Source, Argonne National Laboratory, Argonne, IL, USA. \*e-mail: [yuziliu@anl.gov](mailto:yuziliu@anl.gov); [rajh@anl.gov](mailto:rajh@anl.gov)

**Supplementary Information for**

**Facet-Dependent Active Sites of a Single Cu<sub>2</sub>O Particle Photocatalyst  
for CO<sub>2</sub> Reduction to Methanol**

**Yimin A. Wu<sup>1,2</sup>, Ian McNulty<sup>1</sup>, Cong Liu<sup>3</sup>, Kah Chun Lau<sup>4,5</sup>, Qi Liu<sup>6</sup>, Arvydas P. Paulikas<sup>4</sup>, Cheng-Jun Sun<sup>7</sup>, Zhonghou Cai<sup>7</sup>, Jeffrey R. Guest<sup>1</sup>, Yang Ren<sup>7</sup>, Vojislav Stamenkovic<sup>4</sup>, Larry A. Curtiss<sup>4</sup>, Yuzi Liu<sup>1</sup>, Tijana Rajh<sup>1</sup>**

<sup>1</sup> Center for Nanoscale Materials, Argonne National Laboratory, Argonne, IL 60439, USA.

<sup>2</sup> Department of Mechanical and Mechatronics Engineering and Waterloo Institute for Nanotechnology, University of Waterloo, Waterloo, ON, N2L 3G1, Canada

<sup>3</sup> Chemical Sciences and Engineering Division, Argonne National Laboratory, Argonne, IL, 60439, USA

<sup>4</sup> Materials Science Division, Argonne National Laboratory, Argonne, IL, 60439, USA

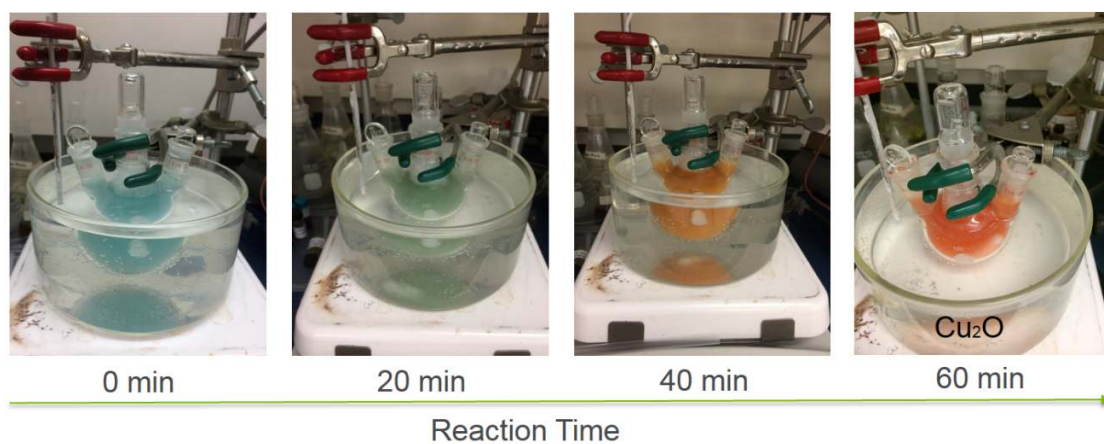
<sup>5</sup> Department of Physics and Astronomy, California State University, Northridge, CA, 91330, USA

<sup>6</sup> Department of Physics, City University of Hong Kong, Kowloon, Hong Kong, China

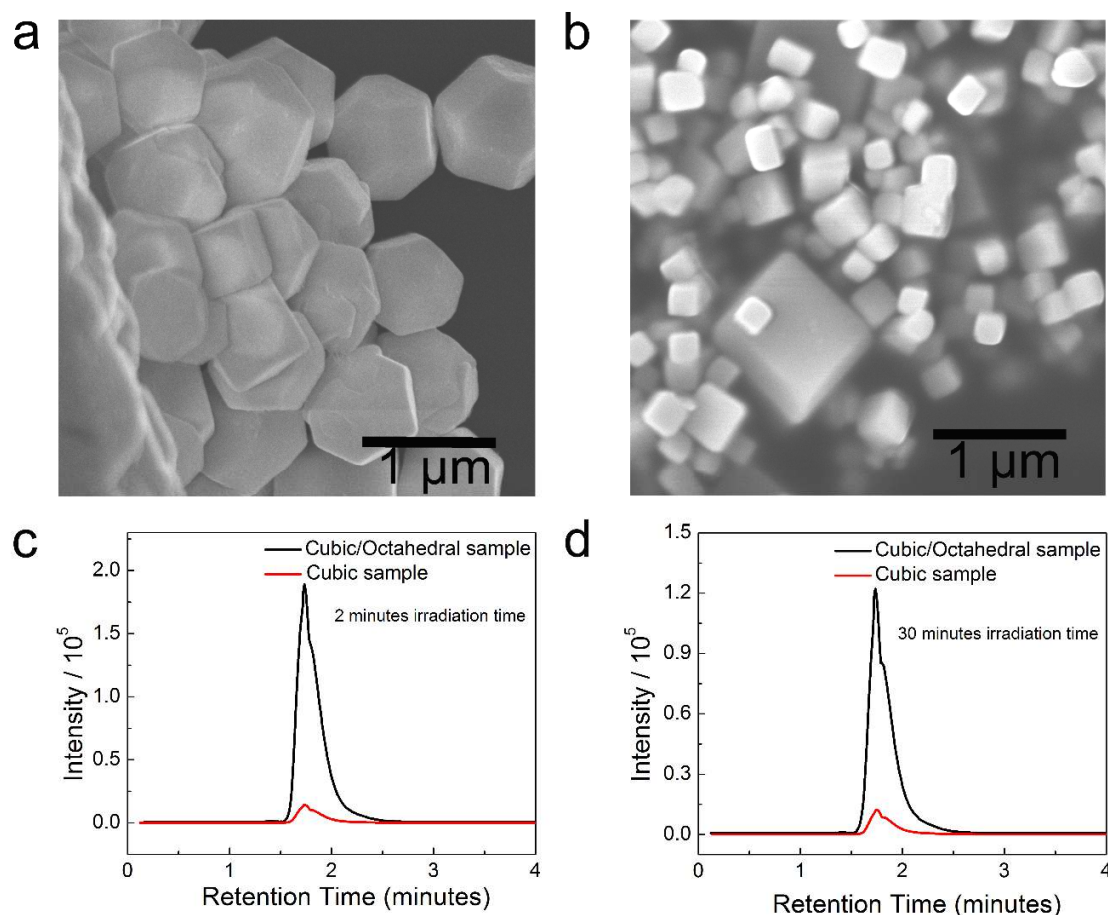
<sup>7</sup> Advanced Photon Source, Argonne National Laboratory, Argonne, IL 60439, USA.

**This Supplementary Information file includes:**

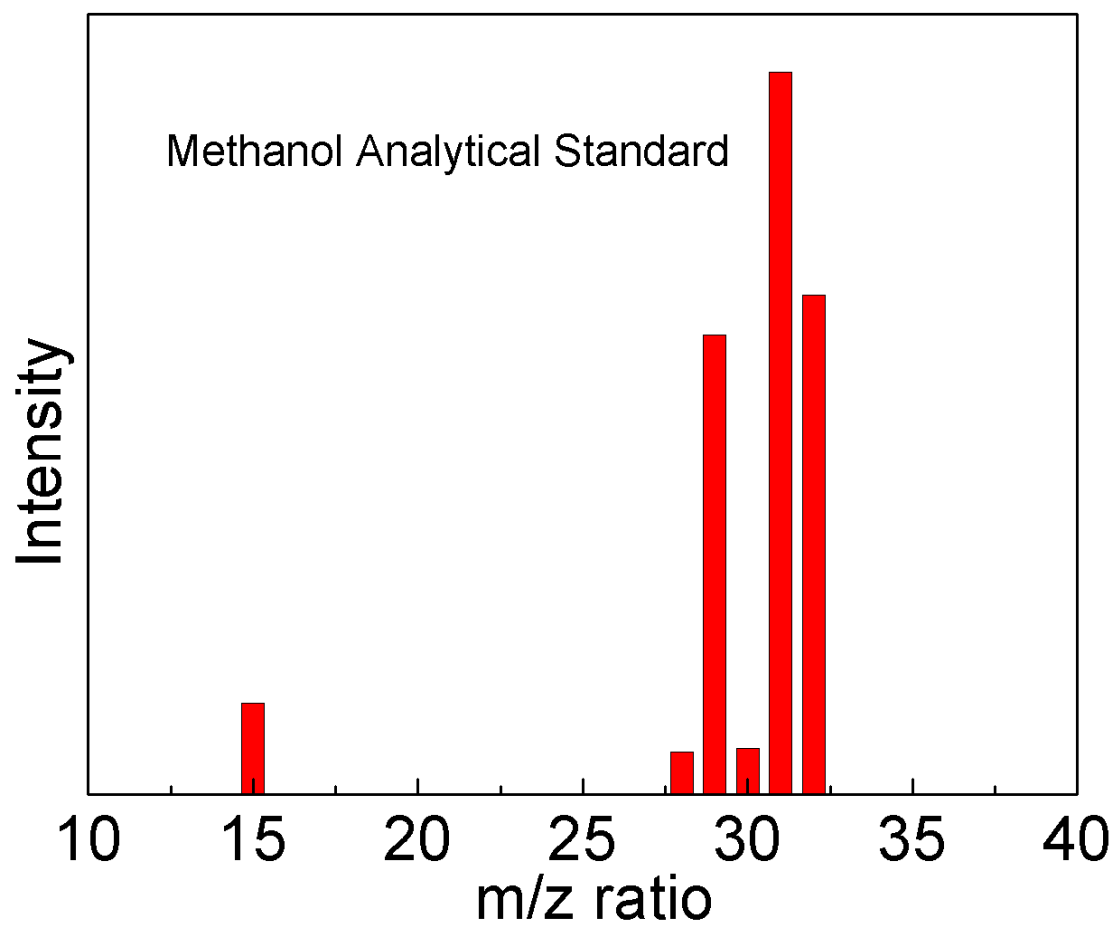
**Figures S1 to S23 and Table 1:**



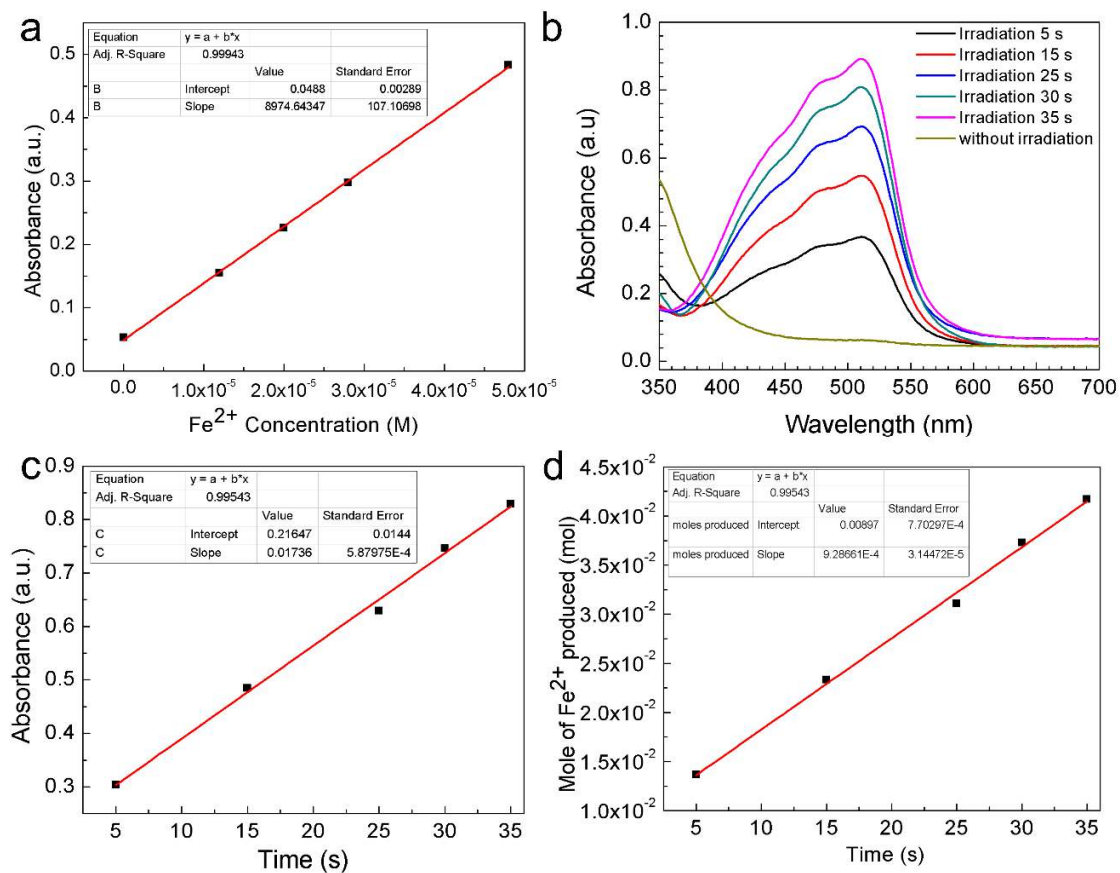
**Supplementary Figure 1 | Illustration of the  $\text{Cu}_2\text{O}$  particle synthesis method.** The solution color changed from blue to green, to yellow, and finally turned brick red with time.



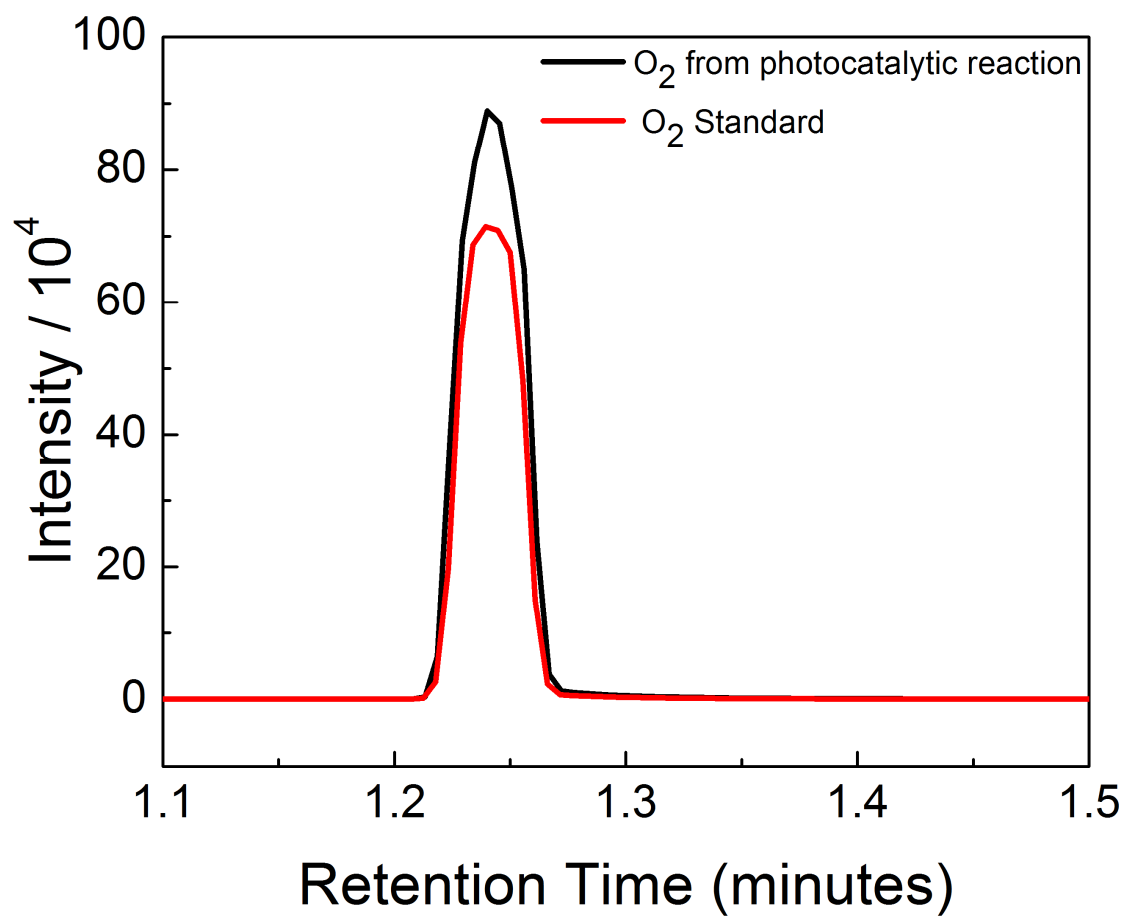
**Supplementary Figure 2 | SEM images and GC results from the two Cu<sub>2</sub>O particle samples.** (a) SEM image of the cubic/octahedral sample. (b) SEM image of the cubic sample. (c) Methanol production by the cubic/octahedral sample (black curve) vs. the cubic sample (red curve), measured by GC after 2 min irradiation time. (d) Methanol production by the cubic/octahedral sample (black curve) vs. the cubic sample (red curve), measured by GC after 30 min irradiation time. The area integrated under the curve obtained with the cubic sample decreased 91% for the 2-min sample and 89% for the 30-min sample, by comparison to the cubic/octahedral sample. This indicates the cubic/octahedral sample, with its larger number of truncations and high-index facets, was more photocatalytically active than the cubic sample.



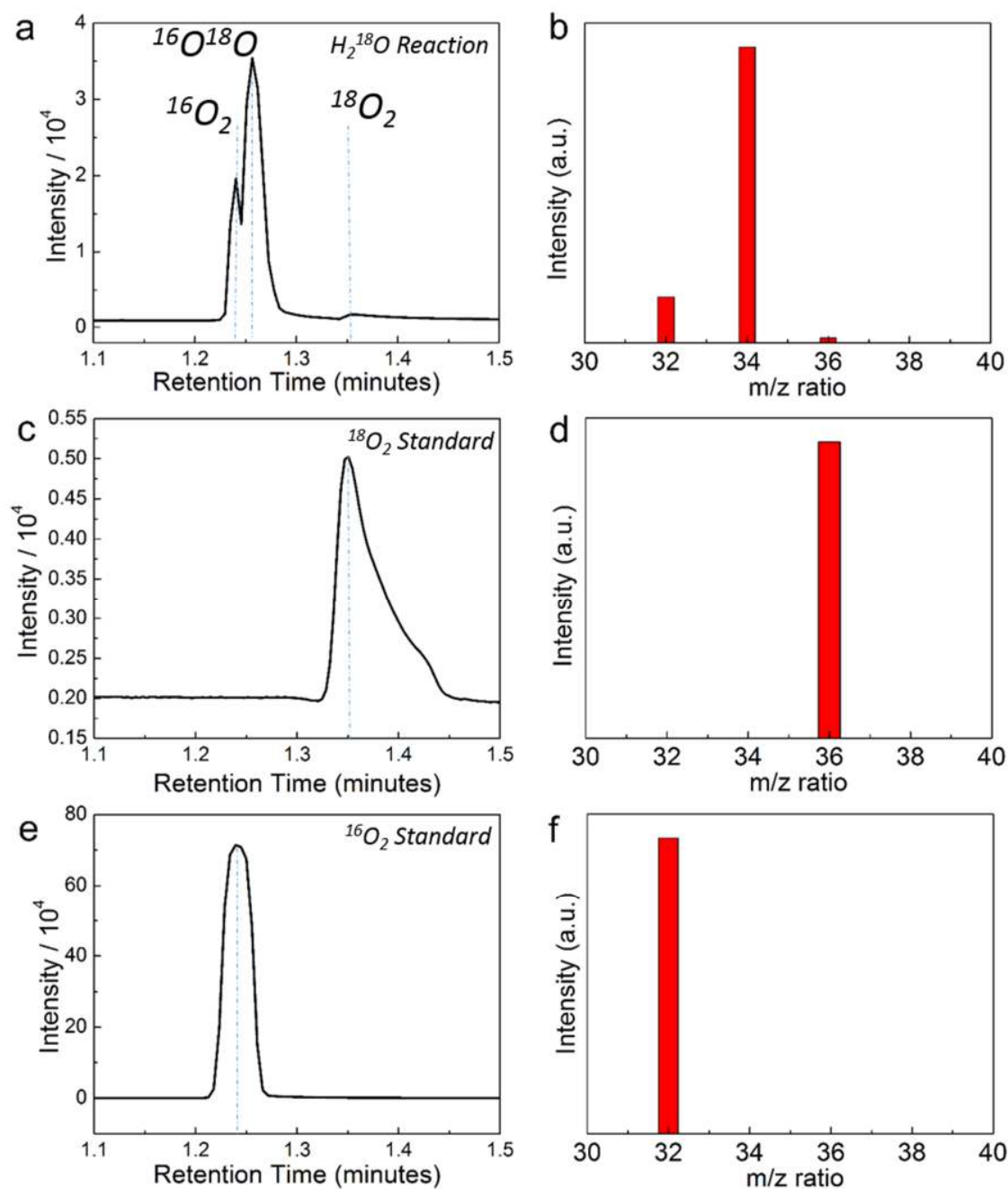
**Supplementary Figure 3 | Mass spectra of a methanol analytical standard.** This was measured using the same instrument and parameter for GC/MS analysis of the photocatalytic products, as in Figure 1.



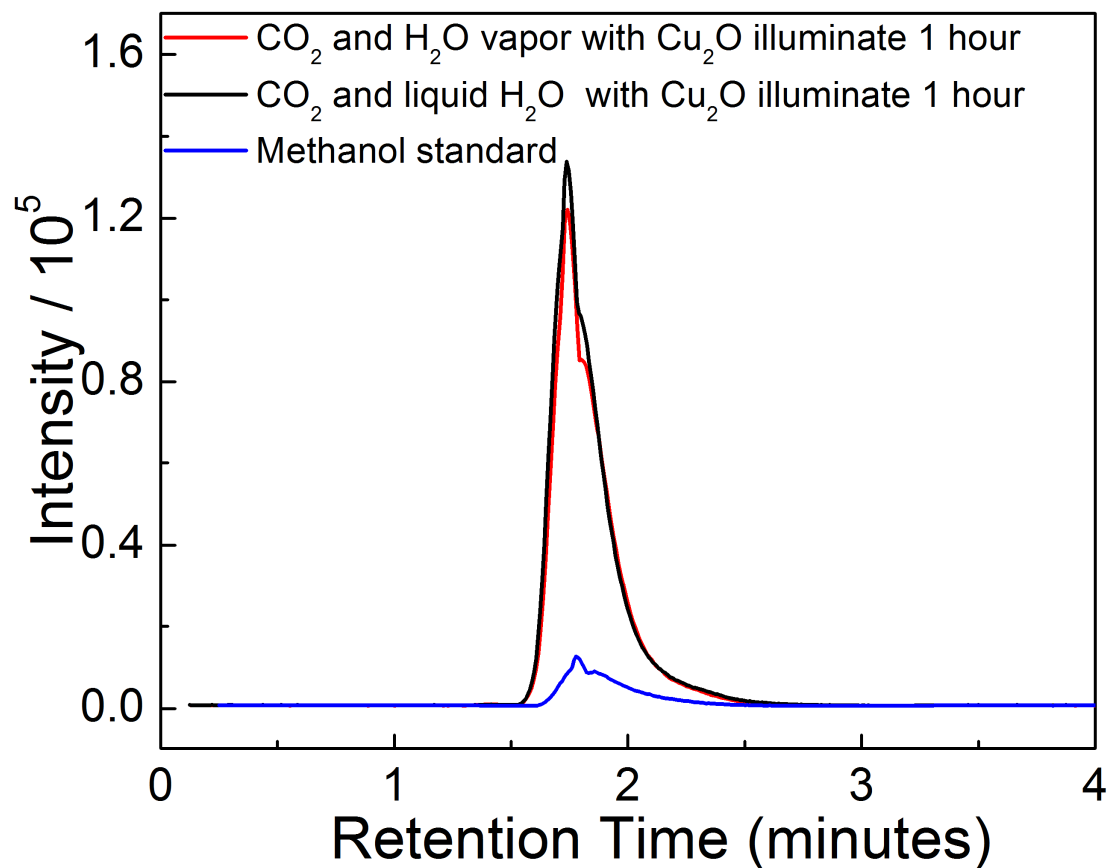
**Supplementary Figure 4 | Actinometry to determine the photon flux from the white light source, which was used for photocatalytic performance measurement. (a)** Molar absorptivity of  $[\text{Fe}(\text{phen})_3]^{2+}$ . **(b)** Irradiation time dependent UV-vis-absorption spectra of produced  $[\text{Fe}(\text{Phen})_3]^{2+}$  from  $[\text{Fe}(\text{C}_2\text{O}_4)_3]^{3-}$  photochemical reaction. **(c)** The absorbance at 510 nm extracted from (b). **(d)** Mole of  $\text{Fe}^{2+}$  produced by the  $[\text{Fe}(\text{C}_2\text{O}_4)_3]^{3-}$  photochemical reaction as a function of irradiation time.



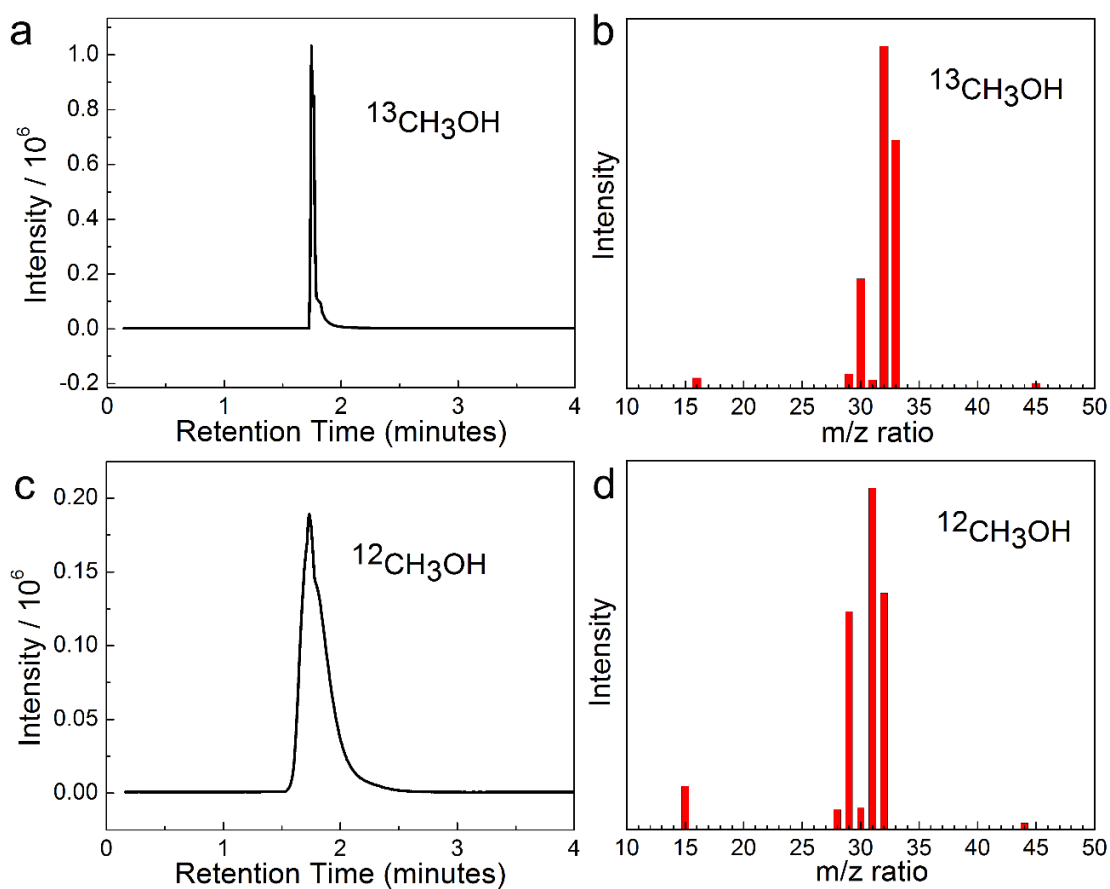
**Supplementary Figure 5 | GC analysis to quantification of oxygen in the photocatalytic reaction after 2 min irradiation time.**



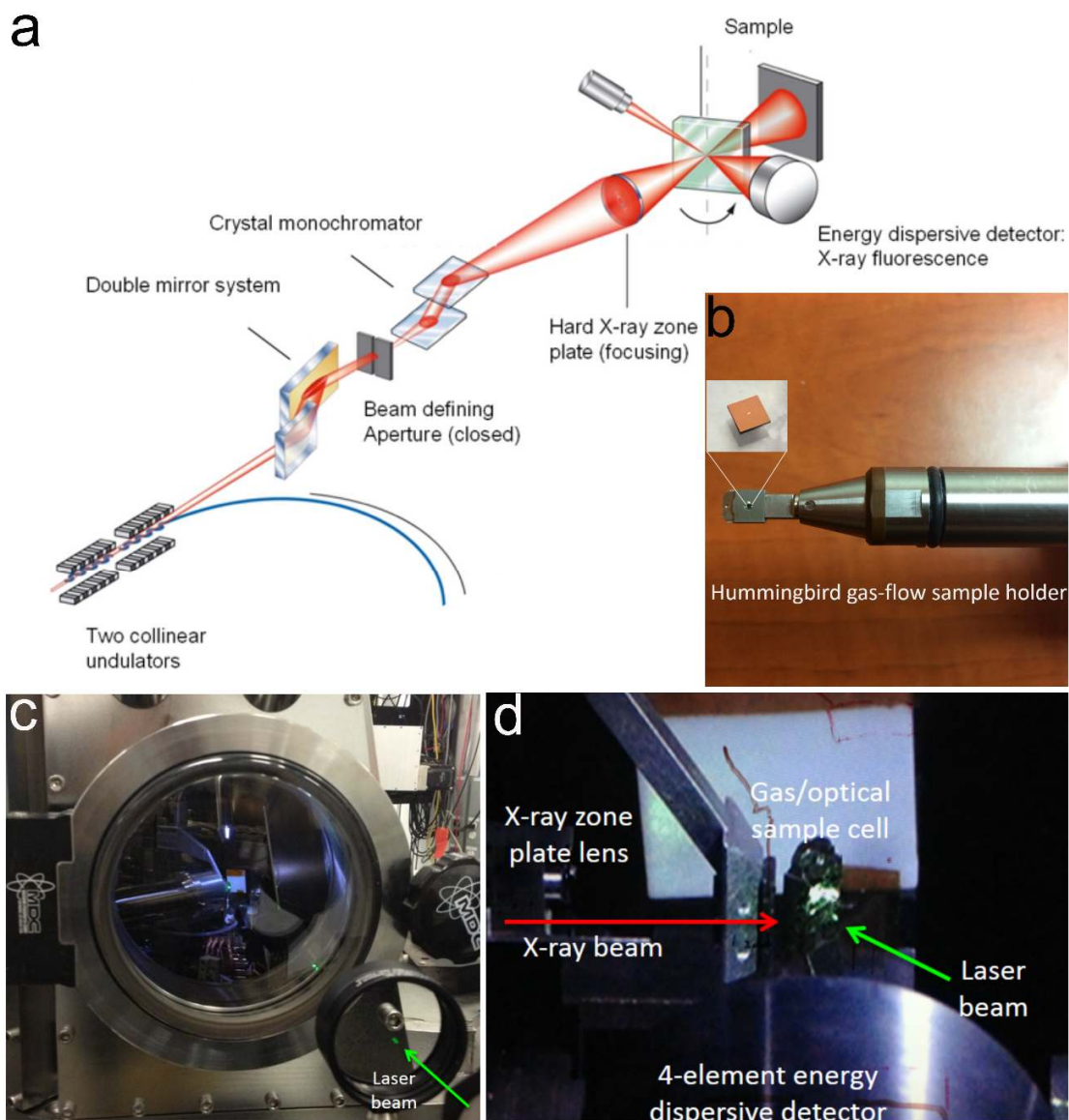
**Supplementary Figure 6 | Oxygen isotope tracer measurement.** (a) Oxygen production from photocatalytic reaction using  $H_2^{18}O$  and  $^{13}C^{16}O_2$  with  $Cu_2^{16}O$ , measured by GC after 2 min irradiation time. (b) Mass spectra of oxygen obtained by GC/MS analysis of (a). Peaks at 32, 34, 36 correspond to  $^{16}O_2$ ,  $^{16}O^{18}O$ , and  $^{18}O_2$ . (c) GC of  $^{18}O_2$  standard. (d) Mass spectra of (c). (e) GC of  $^{16}O_2$  standard. (f) Mass spectra of (e).



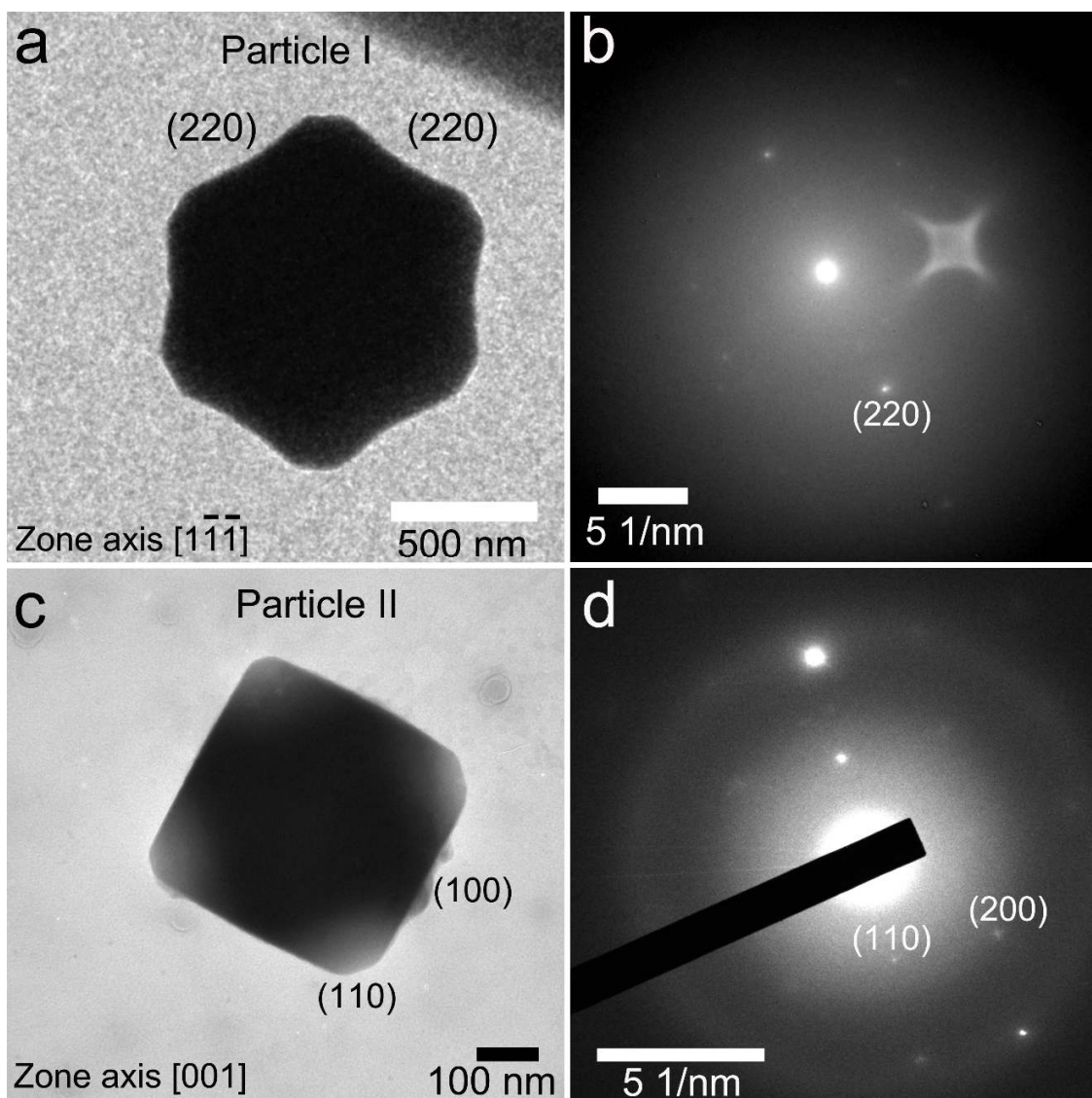
**Supplementary Figure 7 | Comparison of methanol production using H<sub>2</sub>O vapor or liquid H<sub>2</sub>O. GC measurement using CO<sub>2</sub> and H<sub>2</sub>O vapor/liquid H<sub>2</sub>O with Cu<sub>2</sub>O photocatalyst illuminated for 1 hour.** It showed the quantity of methanol production using H<sub>2</sub>O vapor and H<sub>2</sub>O liquid is very similar. This indicates the same reaction mechanism using either H<sub>2</sub>O or liquid H<sub>2</sub>O. The liquid H<sub>2</sub>O produces slightly more methanol than H<sub>2</sub>O vapor. This is due to the slight difference in amount of H<sub>2</sub>O molecules adsorbed on Cu<sub>2</sub>O in H<sub>2</sub>O vapor or in liquid H<sub>2</sub>O.



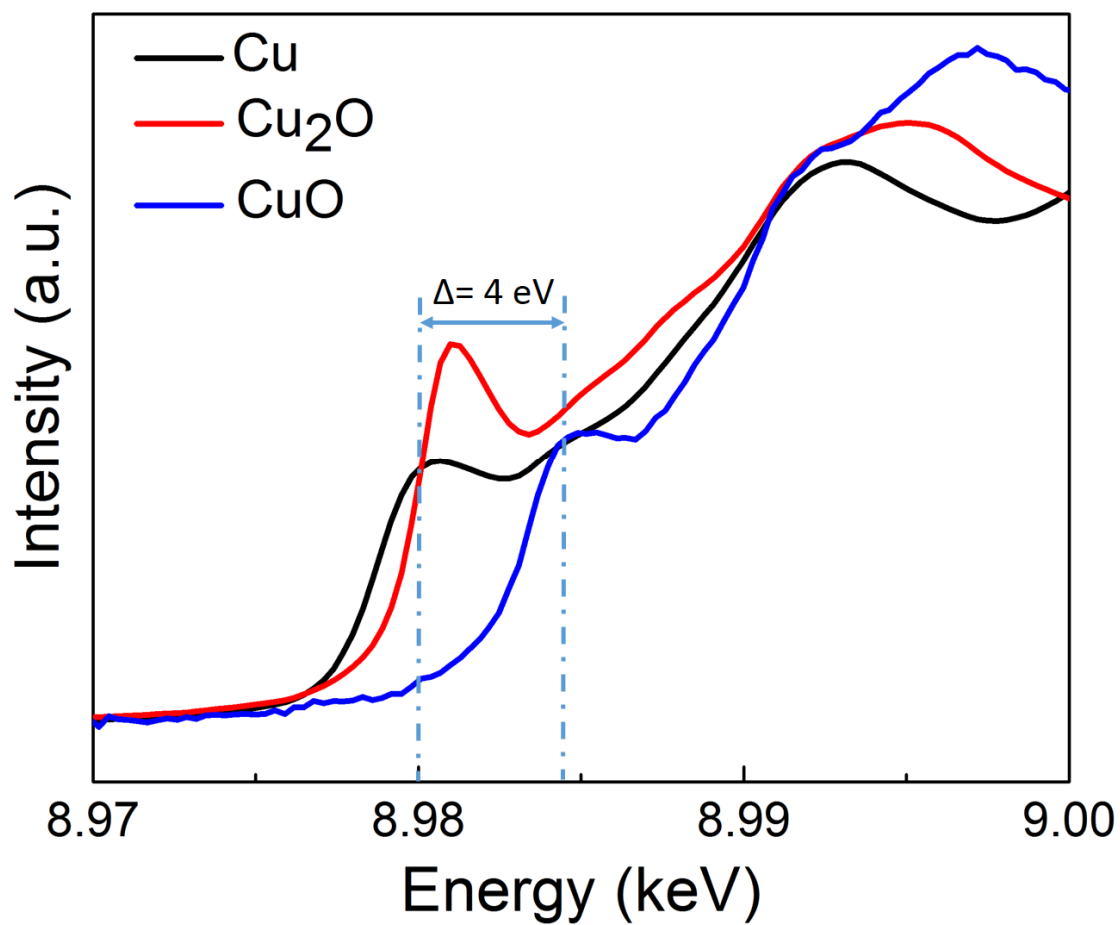
**Supplementary Figure 8 | Carbon isotope tracer measurement.** (a)  $^{13}\text{CH}_3\text{OH}$  production by the cubic/octahedral sample measured by GC after 2 min irradiation time. The retention time was 1.74 min. (b) Mass spectra of methanol obtained by GC/MS analysis of the photocatalytic reaction products from  $^{13}\text{CO}_2$ . Distinct peaks at 16 and 33 were observed with no peak at mass 28. The mass-to-charge ratio of 45 corresponds to unreacted  $^{13}\text{CO}_2$ . (c)  $^{12}\text{CH}_3\text{OH}$  production by the cubic/octahedral sample measured by GC after 2 min irradiation time. The retention time was 1.74 min. (d) Mass spectra of methanol obtained by GC/MS analysis of the photocatalytic reaction products from  $^{12}\text{CO}_2$ . The mass- to-charge ratio of 44 corresponds to unreacted  $^{12}\text{CO}_2$ .



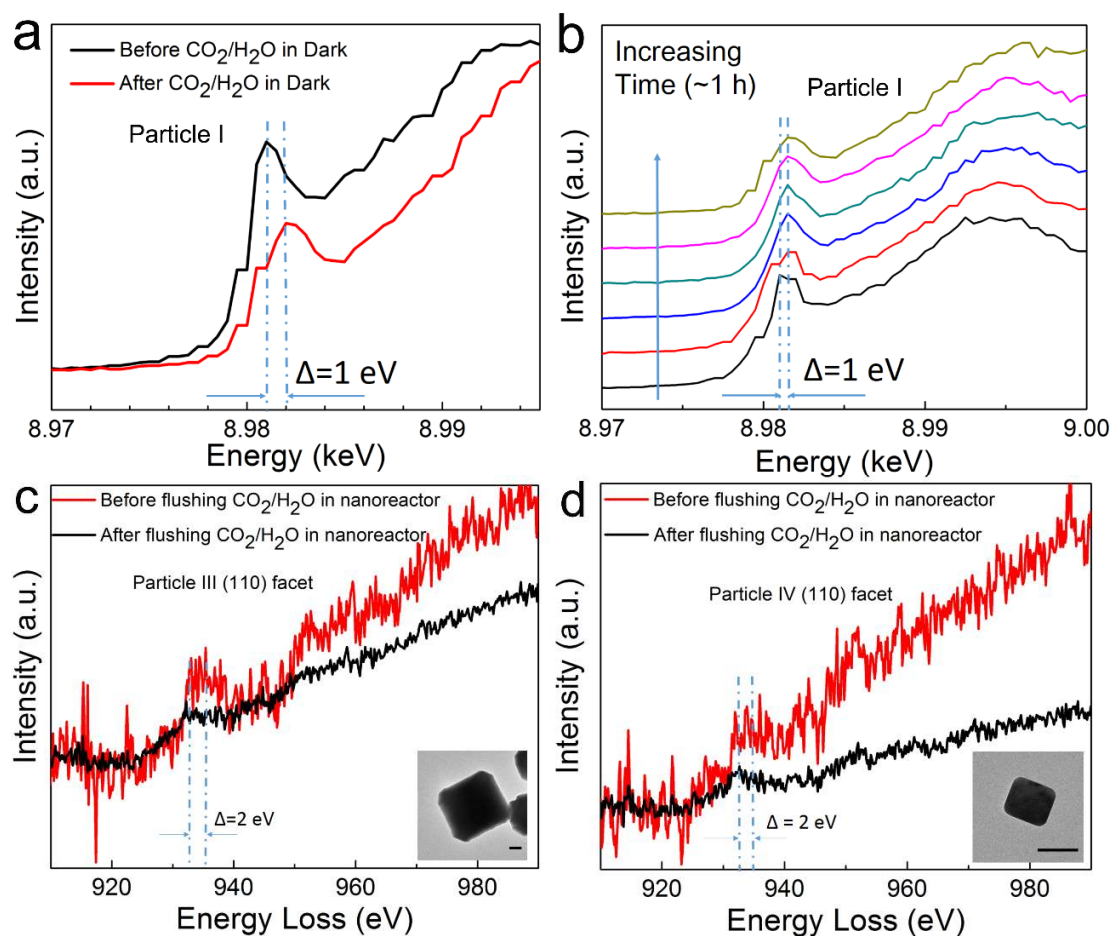
**Supplementary Figure 9 | Scanning fluorescence x-ray microscopy and nanospectroscopy experiment.** (a) Hard X-ray Nanoprobe at CNM/APS beamline 26-ID-C. (b) Cross-platform sample holder and nanoreactor for both TEM and SFXM. (c) Laser setup for *operando* SFXM measurements. (d) View inside the Hard X-ray Nanoprobe, showing the nanoreactor (gas/optical sample cell) x-ray beam path, x-ray zone plate lens, energy-dispersive fluorescence detector, and incident laser beam.



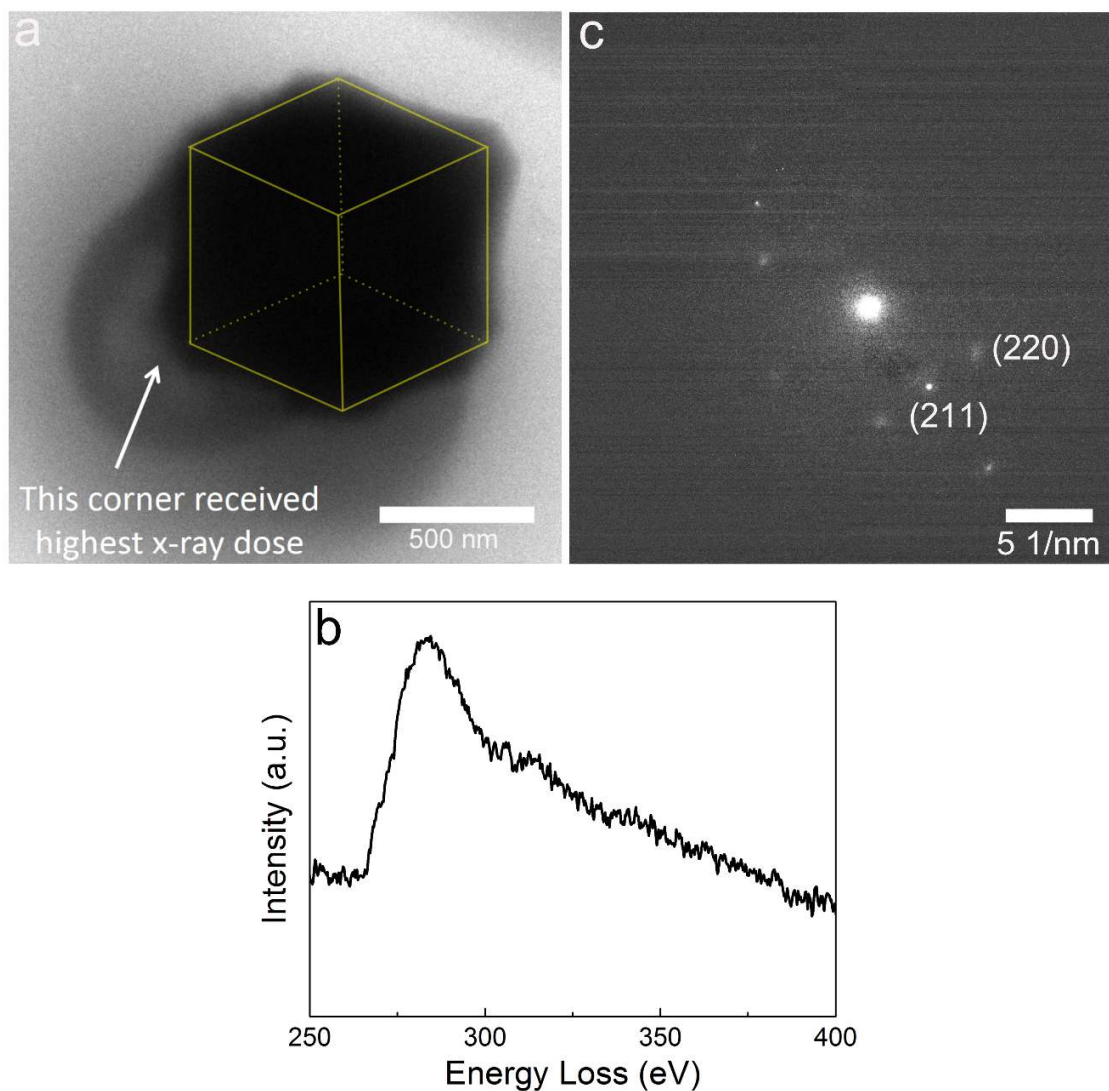
**Supplementary Figure 10 | TEM and Corresponding SPED measurements.** (a) TEM of particle I. (b) SPED data from particle I. (c) TEM of particle II. (d) SPED data from particle II.



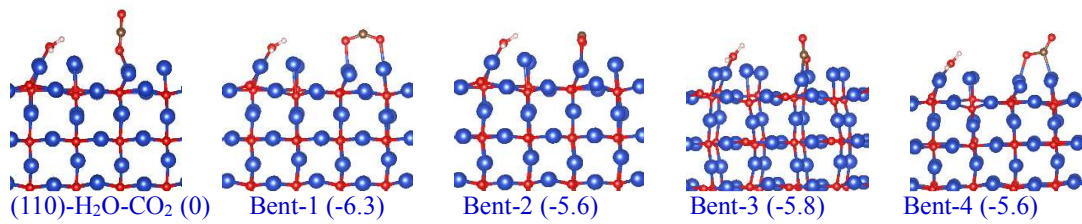
**Supplementary Figure 11 | Reference XAS spectra from standard commercialized powders** (Sigma Aldrich), taken at APS beamline 20-ID-B. The observed shift of the rising Cu K-edge between the metallic Cu and CuO spectra is  $\sim 4 \text{ eV}$ .



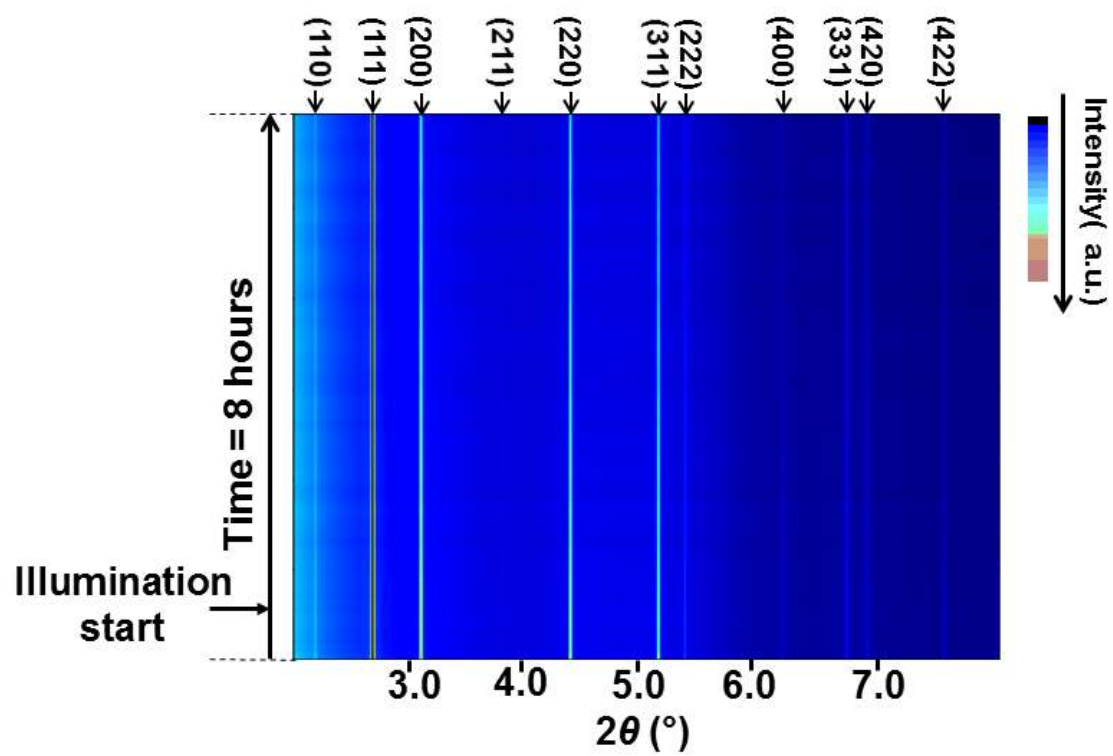
**Supplementary Figure 12 | Additional x-ray nanospectroscopy spectra and EELS spectra.** (a) Spectral shift due to CO<sub>2</sub> adsorption from the (110) facet of particle I as measured by x-ray nanospectroscopy. (b) Time-resolved x-ray point spectra from the (110) facet of particle I recorded at 10 min intervals with the induction of CO<sub>2</sub>/H<sub>2</sub>O gas mixture in the dark state. (c, d) Additional EELS spectra on particle III and particle IV (110) facet before and after flushing CO<sub>2</sub>/H<sub>2</sub>O into the nanoreactor. The lower signal-to-noise ratio with gas at atmospheric pressure is due to greater electron scattering by comparison to TEM column pressure at 10<sup>-6</sup> Pa. Inset shows the corresponding TEM images of particle III and particle IV. The scale bar is 200 nm.



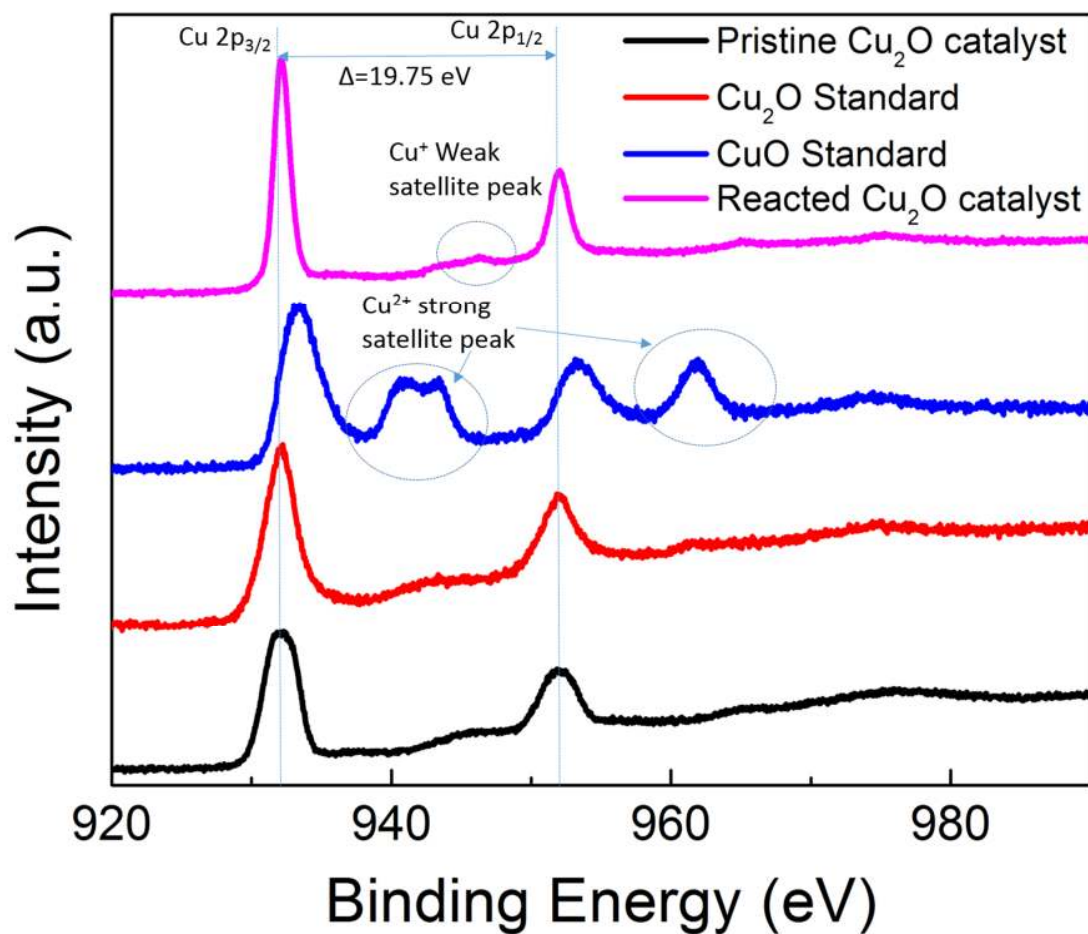
**Supplementary Figure 13 | Analysis of potential x-ray beam effects. (a)** TEM image of particle I as in Figure 2 after the SFXM measurements. **(b)** Some carbon deposition, determined by the presence of a carbon K-edge peak at 284 eV using EELS, was observed near the location that experienced the greatest x ray radiation dose, indicated in (a). **(c)** No obvious structural damage was observed, which was confirmed by SPED.



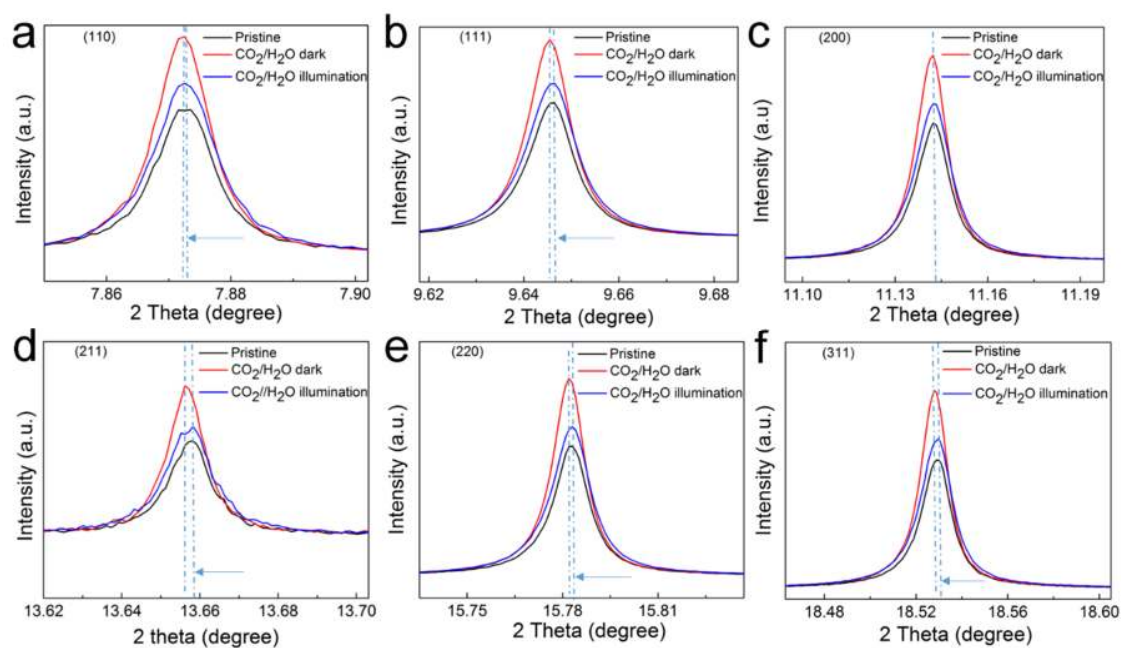
**Supplementary Figure 14 | DFT figure of several "bent" CO<sub>2</sub> when co-adsorbed with H<sub>2</sub>O on Cu<sub>2</sub>O (110)-surface.** Calculated conformations of linear and bent CO<sub>2</sub> (i.e. activated CO<sub>2</sub>)<sup>75</sup> on Cu termination of Cu<sub>2</sub>O (110) with the coadsorption of H<sub>2</sub>O. The numbers in the parentheses are the relative total energies in eV.



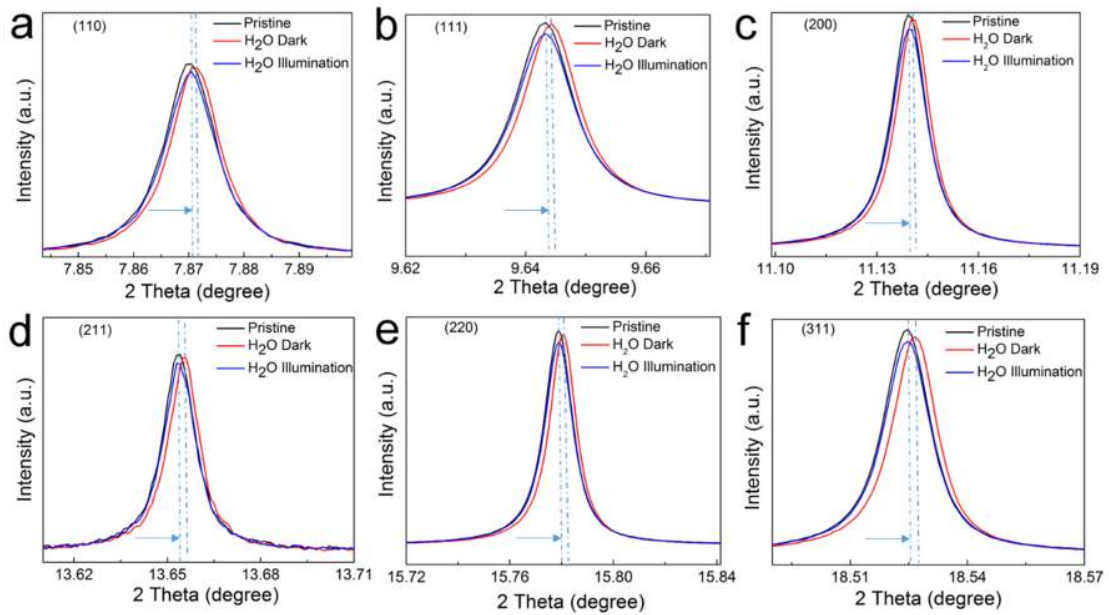
**Supplementary Figure 15 | Structural stability of  $\text{Cu}_2\text{O}$  photocatalyst** during the first 8 h of the photocatalytic reaction on  $\text{Cu}_2\text{O}$  as measured by *operando* HEXRD at APS beamline 11-ID-C.



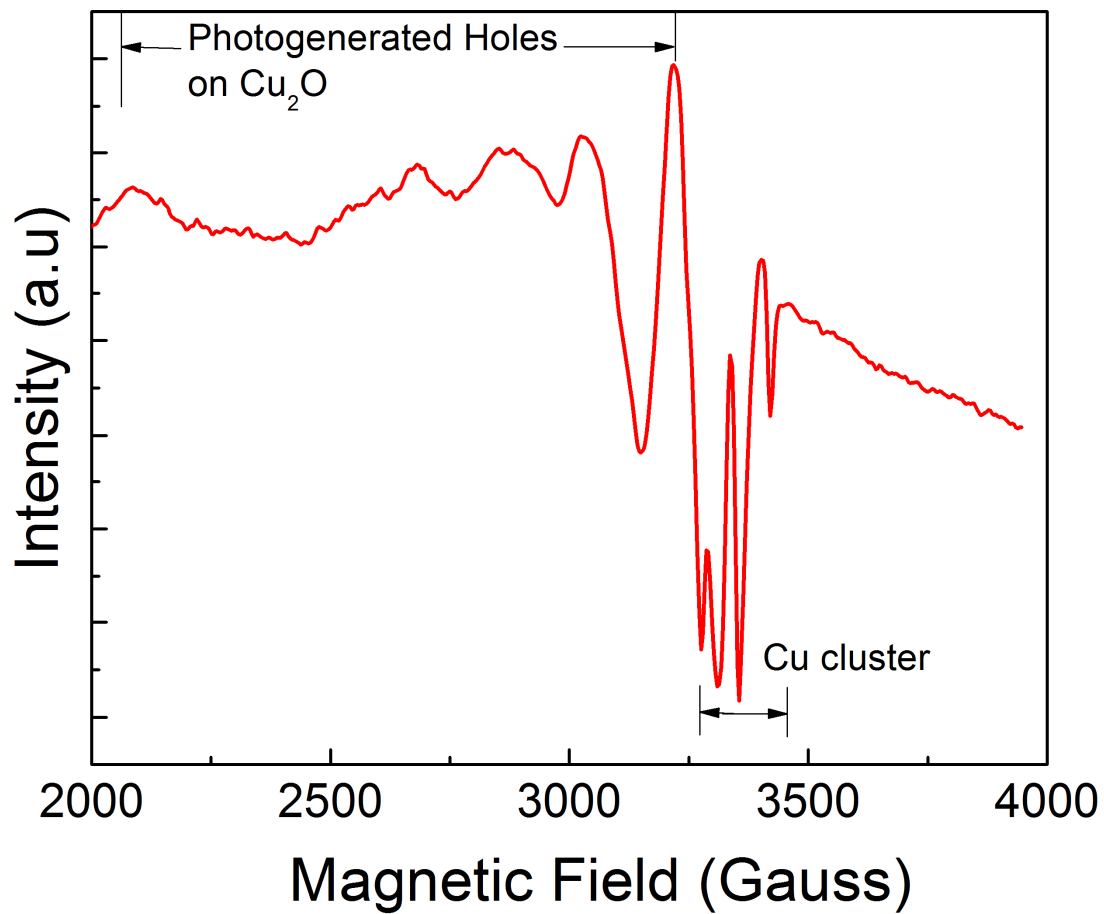
**Supplementary Figure 16 | The stability of Cu<sub>2</sub>O catalyst by *ex situ* x-ray photoemission spectroscopy measurement.** Cu<sub>2</sub>O Cu 2p peak has significant split spin-orbit components ( $\Delta=19.75$  eV, intensity ratio=0.508). It is possible to distinguish Cu oxidation states using satellite features of Cu 2p. CuO has observed collection of strong satellite features around 943 eV while Cu<sub>2</sub>O has weak satellite features around 945 eV. We do not see strong satellite peak in both pristine and reacted Cu<sub>2</sub>O catalyst around 943 eV. This confirms the stability of Cu<sub>2</sub>O catalyst.



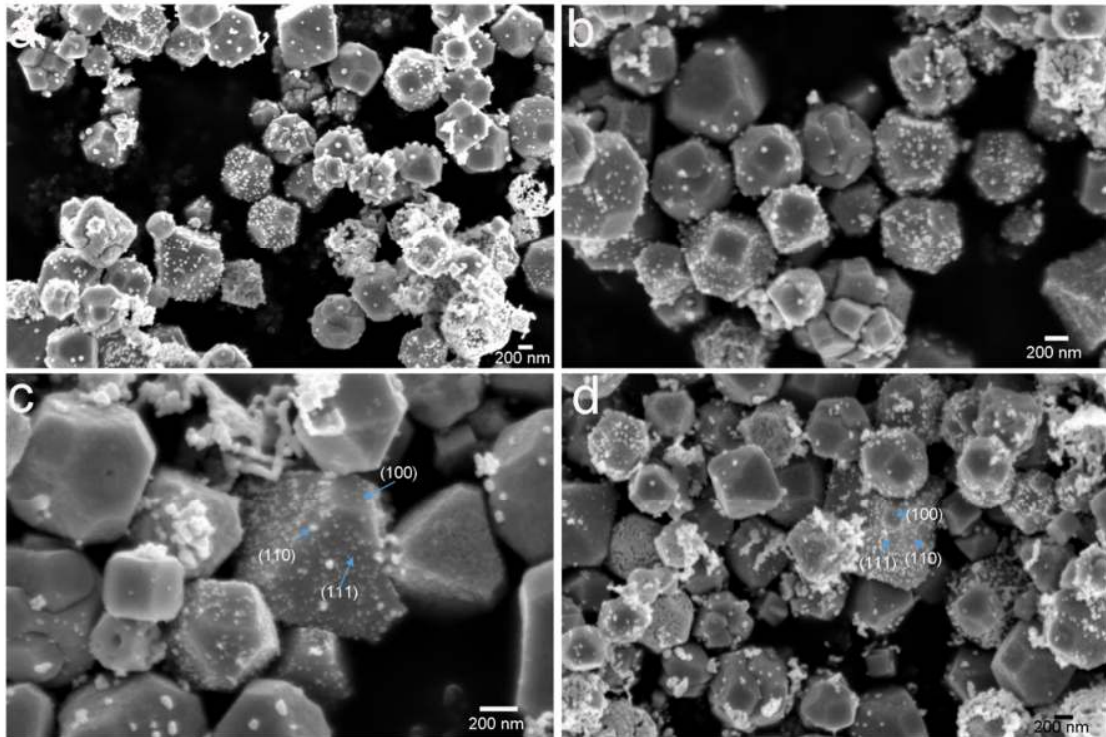
**Supplementary Figure 17 | *Ex-situ* HRXRD measurements of the cubic/octahedral Cu<sub>2</sub>O sample with a CO<sub>2</sub>/H<sub>2</sub>O gas mixture.** All reflections showed lattice expansion (decrease of theta) upon CO<sub>2</sub>/H<sub>2</sub>O adsorption in the dark then and contraction upon illumination. The fraction of Cu atoms near the particle surfaces exposed to gas coadsorption, relative to the pristine Cu atoms within the particle bulk, is about 2% assuming a penetration depth of ~1 nm into a 300 nm particle with imperfect crystal surfaces. The data in figures. S10-S11 were measured at APS beamline 11-BM-B.



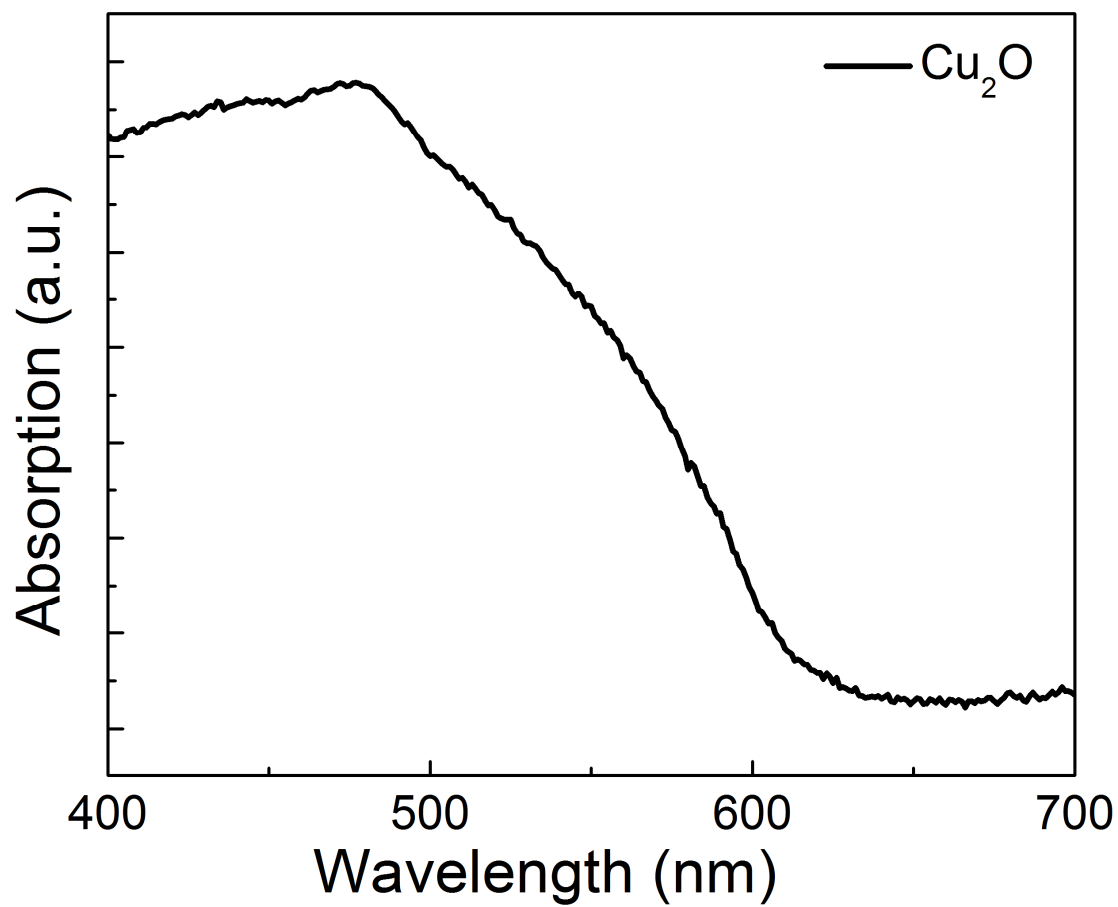
**Supplementary Figure 18 | *Ex-situ* HRXRD measurements of the cubic/octahedral Cu<sub>2</sub>O sample with H<sub>2</sub>O gas alone.** Unlike that with CO<sub>2</sub>/H<sub>2</sub>O gas mixture, adsorption of H<sub>2</sub>O alone by the Cu<sub>2</sub>O crystals led to a decrease in the crystal lattice constant corresponding to lattice contraction (increase of theta).



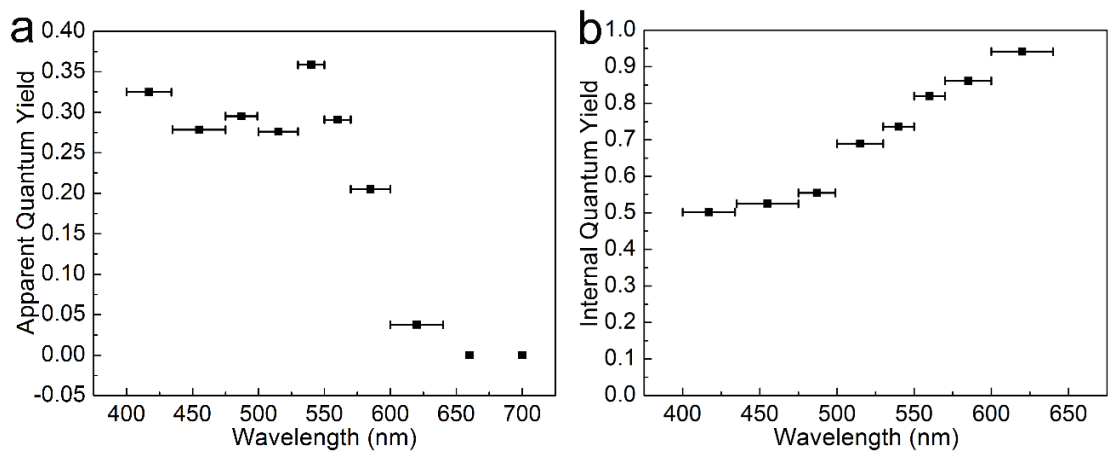
**Supplementary Figure 19 | Additional EPR spectrum.** Illumination of a pristine Cu<sub>2</sub>O crystal produced photogenerated holes and Cu clusters, indicating the synthesized Cu<sub>2</sub>O crystal is a p-type semiconductor, as measured by EPR spectroscopy.



**Supplementary Figure 20 | Photoreduction of H[AuCl<sub>4</sub>] salt to form Au nanoparticles on Cu<sub>2</sub>O particles.** This shows no preferable facets for Au nanoparticles formation from photoreduction. This indicates no charge separation efficiency difference between facets of Cu<sub>2</sub>O.

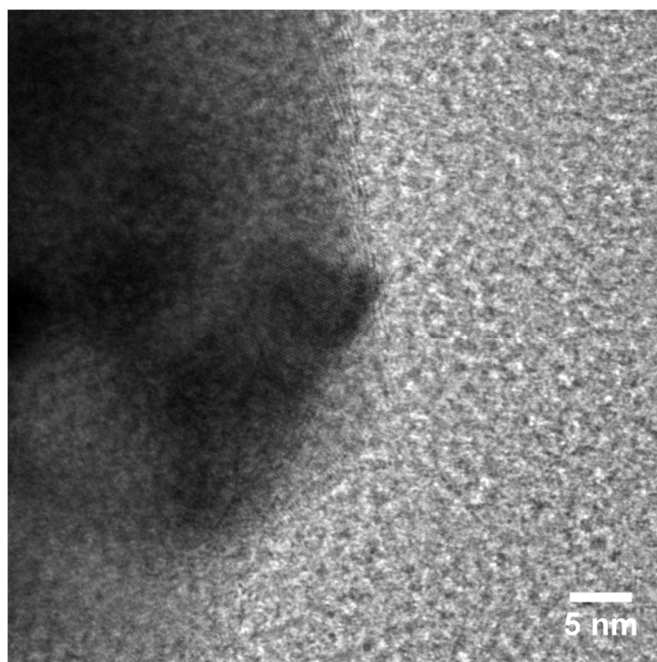


Supplementary Figure 21 | UV-vis-absorption spectrum of cubic/octahedral Cu<sub>2</sub>O.



**Supplementary Figure 22 | Wavelength dependence of apparent quantum yield (a) and internal quantum yield (b) during photocatalytic reduction of CO<sub>2</sub> using Cu<sub>2</sub>O particles. The horizontal bar indicates the wavelength ranges as shown in Supplementary Table 1.**

Table 1, Solar to fuel efficiency calculation					
i	Range (nm)	$\lambda_i$ (nm)	AQY ( $\lambda_i$ ) (%)	P <sub>i</sub> (%)	STF <sub>i</sub> (%)
1	400-435	417	32.4	12	1.5
2	435-475	455	27.8	17	1.9
3	475-500	487	29.5	12	1.5
4	500-530	515	27.6	14	1.8
5	530-550	540	35.8	7	1.2
6	550-570	560	29.0	7	1.0
7	570-600	585	20.4	9	1.0
8	600-640	620	3.7	10	0.2
9	640-680	660	0	8	0
10	680-700	690	0	4	0
Total STF (%)					10.1



**Supplementary Figure 23 | HRTEM image.** A typical HRTEM image of pristine cleaned corners of a Cu<sub>2</sub>O particle.